

Article

A Plastid RNA Polymerase-Associated Protein Is Involved in Early Chloroplast Development in Rice

Shuang Song ^{1,†}, Ying Wang ^{2,†}, Xin Ding ¹, Yunlu Tian ¹, Zewan Wu ¹, Hang Li ¹, Qing Li ¹, Yunpeng Wang ¹, Shirong Zhou ¹, Xiaoou Dong ¹, Jianmin Wan ^{1,3} and Linglong Liu ^{1,*} 

¹ State Key Laboratory for Crop Genetics & Germplasm Enhancement and Utilization, Zhongshan Biological Breeding Laboratory, Jiangsu Plant Gene Engineering Research Center, Jiangsu Plant Gene Editing Engineering Research Center, National Field Scientific Observation and Research Station of Rice Germplasm Resources in Nanjing, Jiangsu, Sanya Research Institute, Nanjing Agricultural University, Nanjing 210095, China

² Vegetable Research Institute, Zhejiang Academy of Agricultural Science, Hangzhou 310022, China

³ National Key Facility for Crop Resources and Improvement, Institute of Crop Science, Chinese Academy of Agricultural Science, Beijing 100081, China

* Correspondence: liulinglong@njau.edu.cn; Tel.: +86-25-84396628

† These authors contributed equally to this work.

Abstract: Plastid-encoded RNA polymerase (PEP) regulates the expression of chloroplast genes involved in photosynthesis and chloroplast development in rice. The PEP-associated protein (PAP) PAP7/pTAC14 is essential for the formation of the PEP complex. However, the function of PAP7 in chloroplast development in rice remains unclear. In this study, we identified a mutant, *w81*, which displays a yellow-green leaf symptom before the four-leaf stage. The seedlings of the *w81* mutant display reduced chlorophyll content, abnormal chloroplast structure, and elevated reactive oxygen species (ROS) level. After the four-leaf stage, plant leaves of the *w81* mutant gradually turn green with increased chlorophyll content. Map-based cloning reveals that the *PAP7* in the *w81* mutant harbors a T to A single-base substitution. This mutation blocks the normal splicing of the fifth intron and generates 74 bp longer transcripts in the mutant. The OsPAP7 protein mainly localizes to the chloroplast and directly interacts with OsPAP5. Our results highlight that OsPAP7 regulates the expression of PEP-dependent chloroplast genes and plays a key role in chloroplast development in rice.

Keywords: rice (*Oryza sativa* L.); chloroplast development; plastid-encoded RNA polymerase (PEP); PEP-associated protein (PAP); OsPAP7



Citation: Song, S.; Wang, Y.; Ding, X.; Tian, Y.; Wu, Z.; Li, H.; Li, Q.; Wang, Y.; Zhou, S.; Dong, X.; et al. A Plastid RNA Polymerase-Associated Protein Is Involved in Early Chloroplast Development in Rice. *Agronomy* **2023**, *13*, 1424. <https://doi.org/10.3390/agronomy13051424>

Academic Editors: Yue Feng and Xiaodeng Zhan

Received: 12 April 2023

Revised: 18 May 2023

Accepted: 19 May 2023

Published: 21 May 2023



Copyright: © 2023 by the authors. Licensee MDPI, Basel, Switzerland. This article is an open access article distributed under the terms and conditions of the Creative Commons Attribution (CC BY) license (<https://creativecommons.org/licenses/by/4.0/>).

1. Introduction

Chloroplasts are the primary organelles responsible for photosynthesis in higher plants. They convert light energy absorbed from the external environment into chemical energy for plant growth and development. Therefore, the normal development of chloroplasts is essential for the growth of a plant. So far, many genes related to the growth and development of chloroplasts have been identified [1–5].

Chloroplast has a nuclear genome which contains two different RNA polymerases (RNAPs). One is a nuclear-encoded RNA polymerase (NEP), and the other is a multi-subunit complex named plastid-encoded RNA polymerase (PEP), which is composed of four core proteins (viz. *rpoA*, *rpoB*, *rpoC1*, and *rpoC2*) [6,7]. The two types of RNAPs have partially overlapping functions, and their relative contributions to plastid expression vary depending on the developmental conditions. NEP is responsible for the expression of housekeeping genes, while PEP is pivotal for the expression of photosynthesis-related genes. According to the recognition sites in NEP and/or PEP promoters, plastidic genes are classified into three types [8–10]. Type I genes are transcribed by PEP, type III by NEP, and type II by both NEP and PEP [11,12]. Previous studies have revealed that NEP functions in

early chloroplast development, and PEP plays a role in mature chloroplasts [10]. In contrast, other studies from barley (*Hordeum vulgare*) or tobacco (*Nicotiana tabacum*) mutants with defective PEP activity have also shown that NEP and PEP are functional at both early and mature stages of chloroplast development [13–16].

PEP often forms a complex with PEP-associated proteins (PAPs). The nuclear genome of *Arabidopsis thaliana* contains at least 12 PAP genes [12,16]. Nowadays, all PAPs have been identified in *Arabidopsis* [17–20]. Previous studies indicated that *Arabidopsis* PAPs play an important role in PEP activity and chloroplast development. In *pap* null mutant plants, the transcription of PEP-dependent genes is reduced, leading to chloroplast developmental defects [21]. There are 10 protein subunits in the PEP complex, which were classified into two different functional groups. One comprises PAP1, PAP2, PAP3, and PAP7, whose domains or motifs (SAP, PPR, S1, SET, respectively) are likely related to gene expression/regulation/enzymic activity, and the other comprises PAP4 to 6 and PAP8 to 10 whose domains or motifs may be involved in redox-dependent processes or regulation [17]. In addition, studies of protein–protein interactions have shown that each PAP interacts with other PAPs or PEP core proteins to form a complex. For example, PAP1/pTAC3 interacts with an α subunit of PEP [22], PAP4/FSD3 interacts with PAP9/FSD2 [23], PAP7/pTAC14 interacts with PAP5/pTAC12 [24], PAP6/FRUCTOKINASE-LIKE PROTEINS1 (FLN1) interacts with PAP10/THIOREDOXIN Z(TrxZ) [25,26], while PAP3/pTAC10 and PAP12/pTAC7 have broad interactions with other PAPs [27,28]. In addition, a previous study demonstrated that PAP2/pTAC2, PAP3/pTAC10, PAP5/pTAC12, and PAP11/MurE play a crucial role in promoting the assembling of the whole PEP complex [29]. Although the above studies increased our understanding of the function of PAPs in plants, the relationship between PAPs and rice chloroplast development and chlorophyll synthesis has not been evaluated.

In this study, we identify the *w81* mutant in rice, which exhibits leaf color change and abnormal chloroplast development at the seedling stage. Map-based cloning reveals that the *W81* locus resides on chromosome 5 and encodes a PAP family member protein. Transgenic experiments verify that the functional deficiency in PAP is responsible for the *w81* mutant phenotype. This study reveals that the *W81* locus is essential for chloroplast development and early-stage seedling growth in rice plants.

2. Materials and Methods

2.1. Plant Materials and Growth Conditions

The *w81* mutant was derived from a mutant bank of *Japonica* cultivar RX69. About 3000 rice seeds from RX69 were irradiated by ^{60}Co ; then, they were cultivated in a field to form M_1 plants. M_2 seeds were separately harvested from each M_1 plant. Then, the M_2 seeds germinated in the field, and the resultant seedlings were screened for leaf color change. The *w81* mutant was identified by its yellow-green leaf symptom before the four-leaf stage. A genetic analysis was conducted by crossing the *w81* mutant and *indica* cultivar yue13. Wild type and the *w81* mutant plants were planted under natural growth conditions in a Rice Station at Nanjing Agricultural University, Nanjing, China. Some of the seedlings for phenotypic observation were planted in a growth chamber (GXM-258B, Ningbo, China) with an ambient temperature of 30 °C and light for 16 h/darkness for 8 h [30].

2.2. Measurement of Chlorophyll Contents

Chlorophyll and carotenoids were measured by referring to the previous methods [31,32]. About 0.03 g of fresh leaves harvested at the three-leaf and heading stages were cut into pieces and soaked in 95% ethanol for 48 h in the dark. After centrifugation, the absorbance of the supernatants was determined by a Hitachi Spectrophotometer (U1800, Hitachi, Tokyo, Japan) at 665, 649 and 470 nm, respectively. There were three replicates per sample of each period.

2.3. Ultrastructural Analysis of Chloroplast

The seedlings from the wild type and *w81* mutant were germinated and grown in a light incubator. The third leaves of 2-week-old plants from the normal green or yellow-green parts of the wild type and *w81* mutant were cut into 0.5 cm² pieces. The cut leaves were completely immersed in 2.5% glutaraldehyde solution after vacuuming. The sample preparation and transmission electron microscopy (TEM) observation were carried out by the Experimental Center of Electron Microscopy, Nanjing Agricultural University. The specific methods were reported in previous articles [33].

2.4. Reactive Oxygen Species (ROS) Detection

The superoxide anions (O²⁻) were detected by nitroblue tetrazolium (NBT), and the hydrogen peroxide (H₂O₂) by diaminobenzidine (DAB) staining. Both O²⁻ and H₂O₂ were cataloged as ROS. The third leaves from the wild type and *w81* mutant at the three-leaf stage were gathered when the yellow-green leaf phenotype was the most obvious. The leaf tissues were soaked in two kinds of dyes, NBT and DAB, respectively, and then the leaves were vacuumed and stained over 12 h at 37 °C in darkness. Lastly, 95% alcohol was used to decolorize the tissues before all green leaves faded.

2.5. Cloning of the W81 Gene

The *w81* mutant (the female parent) was crossed with the *indica* cultivar yue13 (the male parent) for gene mapping. The F₁ generation was self-crossed to obtain the F₂ generation, which was used for gene mapping. A total of 1430 individuals were used to roughly map the *w81* locus. Primer sequences for fine mapping were provided in Table A1. The PCR process included the following steps: 98 °C for 30 s, annealing at 58 °C for 30 s, extension at 72 °C for 40 s, 34 cycles of denaturation-anneal-extension, and finally, extension at 72 °C for 10 min, and preservation at 4 °C.

2.6. Gene Complementation and Knocking out of W81

For the complementation experiments, a 7-kb wild type DNA sequence, including the putative entire coding region, a 2.5-kb upstream sequence, and a 1-kb downstream sequence of LOC_Os05g50980, was inserted into the binary vector pCubi1390. Using the *Agrobacterium tumefaciens* EHA105, the recombinant plasmid pCubi1390-W81 was introduced into the *w81* mutant by the *Agrobacterium*-mediated method [34]. To construct transgenic knockout plants, the targeted W81 guide RNA fragment was designed with the website tool (<http://cbi.hzau.edu.cn/cgi-bin/CRISPR>, accessed on 20 May 2023). The construct was transferred into *Japonica* cultivar Kitaake. The primer details for vector construction are provided in Table A1.

2.7. Subcellular Localization

We amplified the wild type cDNA sequence of the W81 locus and ligated it with the N-terminus of GFP. The recombinant vector was transformed into *Agrobacterium* EHA105, and then tobacco leaves, about 5 to 6 weeks old, were transformed by the *A. tumefaciens*-mediated method [35]. Similarly, the full-length cDNA was inserted into the pAN580 and under the control of the CaMV35S promoter. The resultant vector was transformed into rice protoplasts, as previously reported [36]. The GFP fluorescence signal was observed with a confocal laser scanning microscope (LSM780, Carl Zeiss, Germany) [35]. Subcellular localization primers are shown in Table A1.

2.8. Quantitative Real-Time PCR (qRT-PCR) Analysis

Total RNA was isolated from the *w81* mutant at different illumination times or in different tissues. The extraction procedure followed the manual of an RNA Prep Pure Plant kit (TIANGEN Biotech, Beijing, China). Total RNA (about 2 µg) was treated with Superiorscript Reverse Transcriptase (Enzymatics, <https://www.enzymatics.com>, accessed on 20 May 2023) and oligo(dT) or arbitrary primers for single-strand cDNA synthesis. The

prime sequences of the qRT-PCR are shown in Table A1. In each gene detection, an internal control (*UBQ5*, *ubiquitin5*) was adopted to normalize the qRT-PCR results. The data were processed by a $2^{-\Delta\Delta CT}$ method [30,37].

To detect the *W81/LOC_Os05g50980* transcripts in the *w81* mutant and the wild type, a pair of primers (980-CDS-CUT-1F/1R, Table A1) were designed to amplify the full-length coding sequence via RT-PCR. After PCR amplification, 1.5% agarose gel was prepared to detect the transcript size differences between the *w81* mutant and its wild type.

2.9. Yeast Two-Hybrid Assay

The full-length coding regions of *OsPAP7* and *OsPAP5* were cloned into the pGBKT7 vector as preys. Reverse experiments with *OsPAP7* and *OsPAP5* as baits were conducted simultaneously. In order to carry out the interaction test, each bait construct and each prey construct were co-transformed into the yeast strain AH109, then plated on an SD/-Trp-Leu medium, and kept at 30 °C for 2 days. Afterward, the yeast clones were continuously diluted (1:10, 1:100, 1:1000) and cultured on a selective medium at 30 °C for 4 days. The empty vector was transformed simultaneously as a negative control. The related primers are shown in Table A1.

2.10. Bimolecular Fluorescence Complementation Assay

The full-length cDNA fragments of *OsPAP7* and *OsPAP5* were inserted into pSPYNE173 and Pspycy (M) vectors, respectively. The related primers are shown in Table A1. *Nicotiana benthamiana* leaves were transformed with different combinations of *Agrobacterium*, including the above plasmids, and followed a previous protocol [35]. After 48 h, the YFP signal was detected in leaves by the LSM780 confocal laser scanning microscope.

3. Results

3.1. Phenotypic Analysis of the *w81* Mutant

The yellow-green leaf *w81* mutant was screened and obtained from a ^{60}Co -irradiated mutant collection in the Japonica rice cultivar RX69. The *w81* mutant showed a yellow-green leaf phenotype before the four-leaf stage, with the most obvious symptom detectable in the third leaf (L3) (Figure 1A,B). Afterward, the yellow-green leaf phenotype gradually turned green, and the newly-emerged leaves displayed normal green color from the fourth leaf (L4). Interestingly, the yellow-green leaf phenotype emerged again at the tillering stage (Figure 1C). After the heading stage, no difference was observed between the mutant and its wild type (WT) (Figure 1D). In order to further observe the characteristics of the *w81* mutant, the contents of the chlorophyll and the carotenoid at different periods were determined. At the three-leaf stage, the chlorophyll a and chlorophyll b contents of the *w81* mutant were significantly lower than those of the wild type (WT). At the heading stage, however, there was no significant difference between the contents of chlorophyll a and chlorophyll b of the *w81* mutant and those of the wild type (WT). These physiological results were highly in agreement with the phenotypic change (Figure 1E).

Additionally, some major agronomic traits in the mutant, such as plant architecture (including plant height, number of tillers per plant) and yield-related traits (branch numbers per panicle, number of spikelets per panicle and 1000-grain weight), were measured, and they showed no significant difference from those of the wild type plants (Table A2).

In order to study the effects of the *w81* mutation on chloroplast development, chloroplasts from the *w81* mutant leaves in the three-leaf-stage and wild type seedlings were observed (Figure 2A–D). Compared with the wild type, chloroplast development of the *w81* mutant was incomplete; many osmophilic bodies appeared, and chloroplasts were deformed and irregular (Figure 2A,B). The thylakoid lamellar structure in the chloroplast of the *w81* seedlings was obviously loose, and there was no stacking structure (Figure 2C,D). Therefore, the yellow-green leaf color of the *w81* mutant might be associated with the developmental defects of chloroplasts.

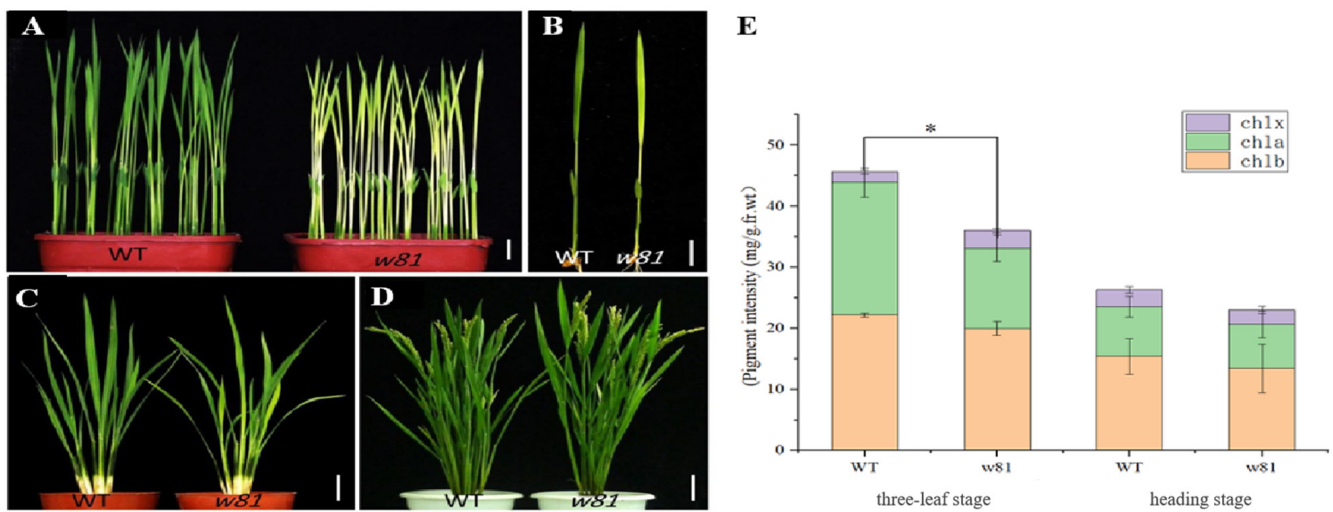


Figure 1. Phenotypic analysis of the wild type and *w81* mutant plants. (A,B) Seedlings of wild type (WT, left) and *w81* mutant (right) at the three-leaf stage. Scale bars = 1 cm. (C) Comparison of leaves of wild type (WT, left) and *w81* mutant (right) plants at the tillering stage. Scale bars = 5 cm. (D) Phenotypes of wild type (WT, left) and *w81* mutant (right) mutant plants after the heading stage. Scale bars = 10 cm. (E) The chlorophyll contents of wild type and *w81* mutant at the three-leaf (left) and heading stages (right). Chl a: Chlorophyll a; Chl b: Chlorophyll b; Chl x: carotenoids; FW: fresh weight. Error bars represent \pm SD ($n = 3$). Asterisks denote a significant statistical difference by Student's *t*-test, * $p < 0.05$.

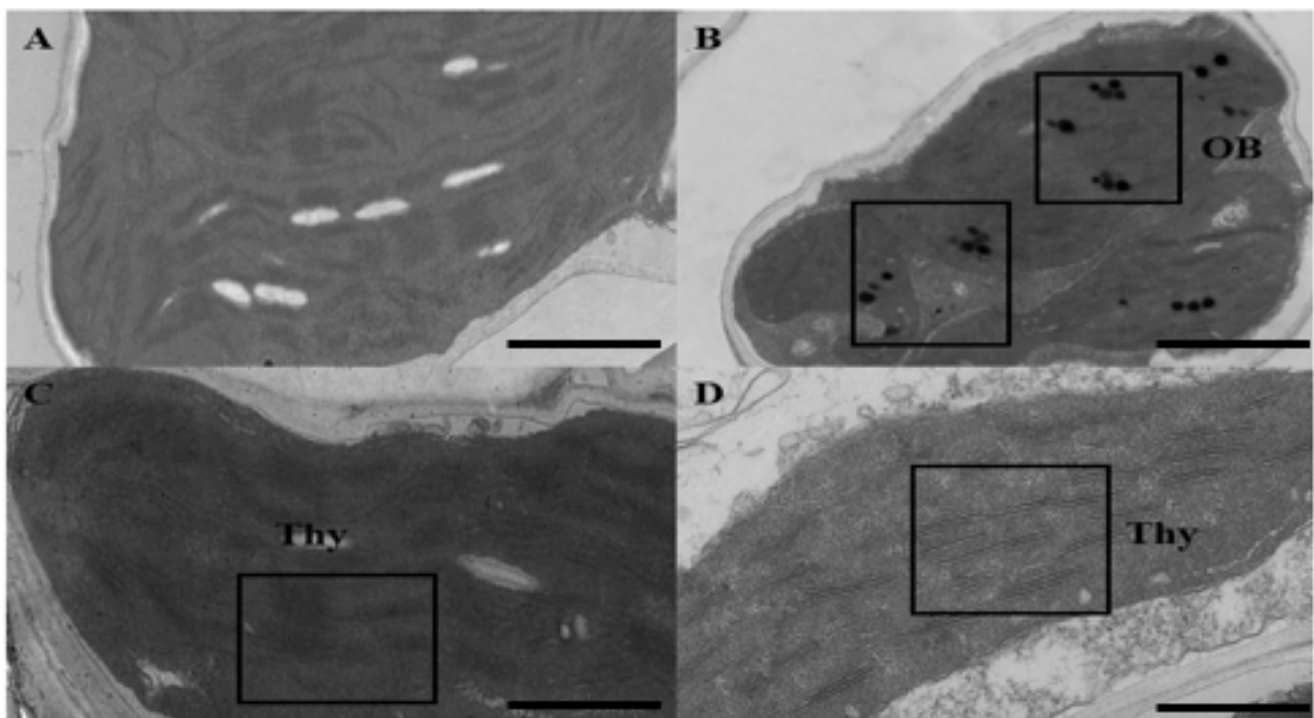


Figure 2. Observation of chloroplasts from the wild type (WT) and *w81* mutant with transmission electron microscope. (A,C) Chloroplast ultrastructure of wild type (WT) leaves at three-leaf stage. (B,D) Chloroplast ultrastructure of *w81* mutant leaves at three-leaf stage. Thy, thylakoid lamellar (in black box); OB, osmophilic body (in black box). Scale bars = 800 nm.

3.2. Analysis of ROS Accumulation in the *w81* Mutant

The change in rice leaf color is mostly a photobleaching phenomenon caused by the excessive accumulation of ROS, which functions as a signal to induce the expression of

oxidation-related genes [38]. In order to detect the accumulation of ROS in the leaves, NBT and DAB staining were conducted to detect $O_2^{\cdot-}$ and H_2O_2 generated from the three-week-old leaves. The NBT staining showed that the *w81* mutant exhibited a higher level of $O_2^{\cdot-}$ accumulation than the wild type (Figure 3A). Similarly, the DAB staining showed that the H_2O_2 activity of the *w81* mutant was higher than that of the wild type (Figure 3B). These results indicated that the *w81* mutant had a certain level of ROS accumulation and could produce photooxidation stress under light stimulation, hence resulting in the photobleaching phenomenon. In addition, qRT-PCR was deployed to analyze the expression of some genes involved in the ROS-scavenging system. The results showed that, except for AOX1a, all other genes were remarkably up-regulated (Figure 3C). These results suggest that the *w81* mutant has a higher level of ROS accumulation, which induces the up-regulation of the expression of genes related to the antioxidant mechanism, thereby ensuring the survival of the plant.

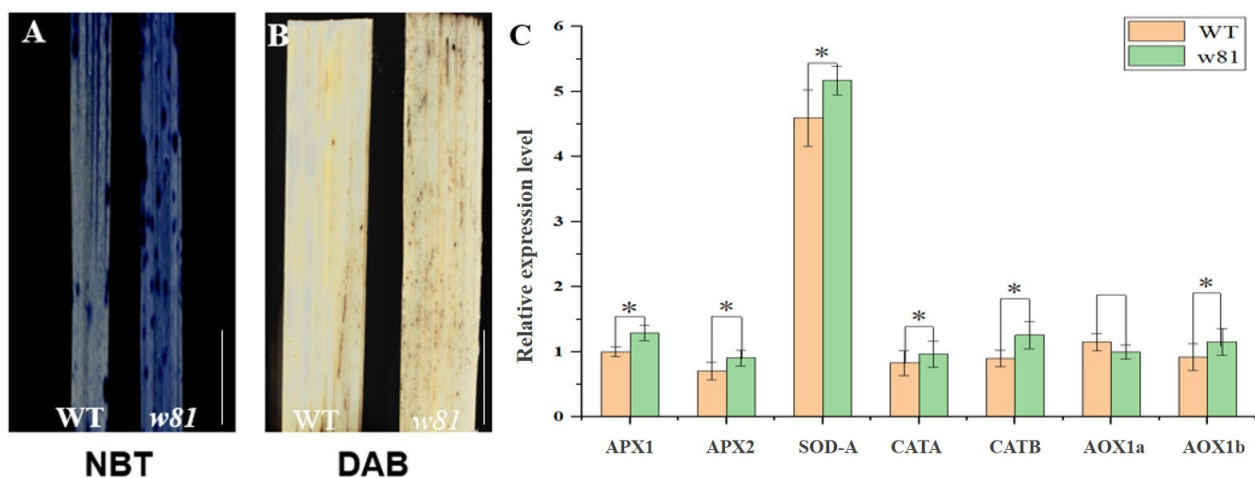


Figure 3. Detection of reactive oxygen species (ROS) activity and expression analysis of ROS scavenging-related genes. (A) Nitroblue tetrazolium (NBT) staining to visualize superoxide anion ($O_2^{\cdot-}$). Scale bars = 1 cm. (B) Diaminobenzidine (DAB) staining to visualize hydrogen peroxide (H_2O_2). Scale bars = 1 cm. (C) qRT-PCR analysis of ROS scavenging-related genes. Error bars represent \pm SD ($n = 3$). The star indicates a significant difference by Student's *t*-test, * $p < 0.05$.

3.3. Map-Based Cloning

Two F_2 populations were produced from the *w81*(female parent) \times RX69(male parent) and RX69(female parent) \times *w81*(male parent), respectively. A genetic analysis showed that the *w81* mutant phenotype was conferred by a single recessive nuclear gene (Table A3). Using the *w81/yue* 13 F_2 population, the *W81* locus was initially mapped on the endpoint of the long arm of chromosome 5, between the markers S5-1 and L5-8 (Figure 4A). With the 1430 F_2 homozygous recessive *w81*-like individuals, the *W81* locus was further mapped on two bacterial artificial chromosome clone sequences (BAC1, OSJNBa0009C07; BAC2, OJ1007_H05) and was ultimately delimited in a 37.5-kb region between the markers S5-19 and S5-3, which included six putative open reading frames (ORFs) (Figure 4B,C). Gene sequencing of all six ORFs between the *w81* mutant and wild type indicated that only the fifth ORF (LOC_Os05g50980) harbors a single-nucleotide change (T \rightarrow A) 7-bp in front of the sixth exon (Figure 4D). This mutation creates a new 3' splicing site (AG), which may disturb or prevent the recognition of the spliceosome in the *w81* mutant. RT-PCR indicated there was an additional longer transcript in the *w81* mutant compared to the wild type (Figure 4E). Sequencing analysis showed that the long transcript in the mutant remained at the 74-bp fifth intron of ORF5 completely (Figure 4F), suggesting the point mutation affects the normal transcript splicing in the *w81* mutant.

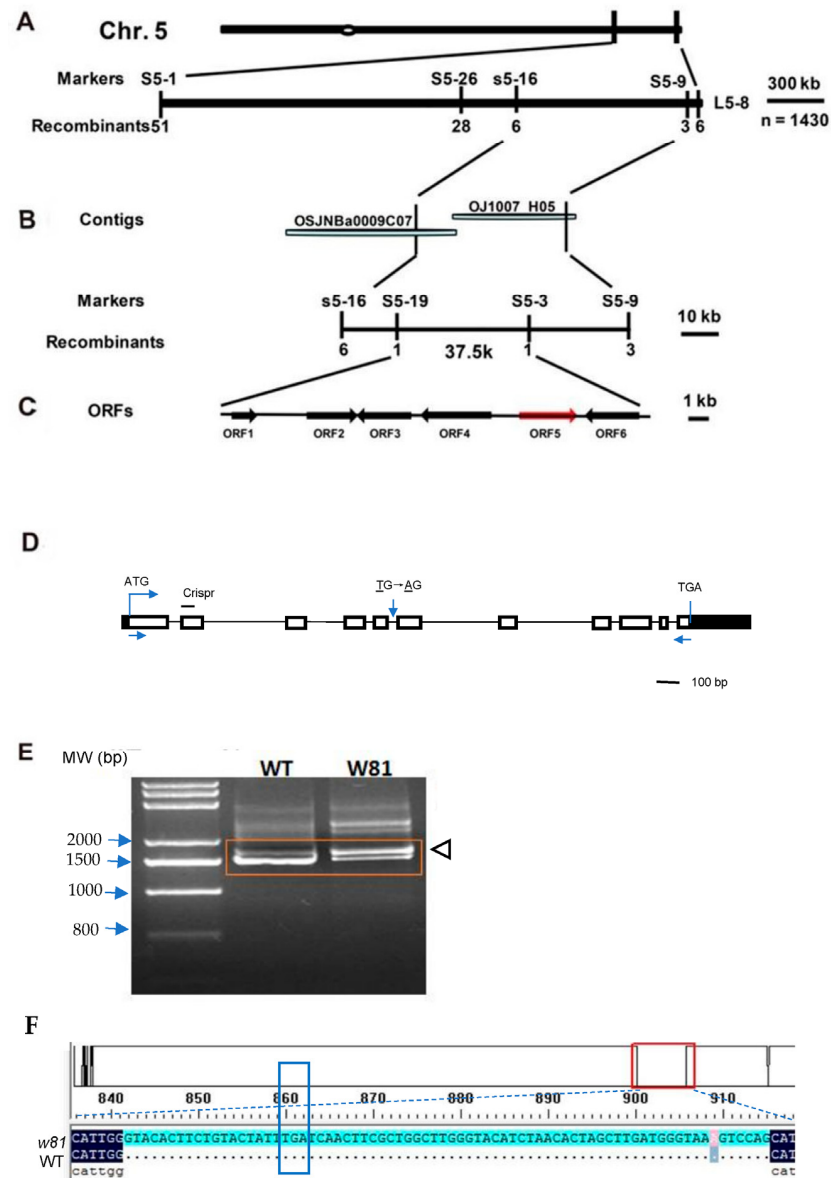


Figure 4. Map-based cloning of the *W81* gene. (A) The *W81* locus was delimited between the markers S5-1 and L5-8. (B) The further position includes two bacterial artificial chromosome clone sequences (BAC1, OSJNBa0009C07; BAC2, OJ1007_H05). The *W81* locus was ultimately mapped to a 37.5-kb region between the markers S5-19 and S5-3 using 1430 F₂ homozygous mutant-like plants. (C) The mapped region contains six predicted open reading frames. Black arrow indicates predicted gene and its transcriptional direction. Red arrow shows a candidate gene and its transcriptional direction. (D) Gene structure of ORF5. The mutation site (T→A, underline) is at the position 7-bp in front of sixth exons (indicated by an arrowhead) and creates a new 3' splicing site (AG). White boxes denote exons, and the lines between them denote introns. Black boxes indicate 5' and 3' untranslated regions (UTR). ATG represents the start codon, and TAG is the stop codon. Arrows below the start and stop codons are primer sites designed for detecting gene transcripts. The site for knocking-out in the CRISPR lines (Crispr) is shown with a line. (E) Detection of transcripts (in box) in *w81* mutant and its wild type. The mis-splicing mutation leads to an additional 74 bp longer transcript in *w81* mutant (triangle) compared with its wild type. MW indicates the nucleotide molecular weight standard. (F) Comparison of transcript sequences between the wild type (WT) and *w81* mutant. The upper panel shows full-length transcript sequences, and lower panel displays only different parts between the WT and *w81* mutant. A putative newly gained stop codon in *w81* mutant is shown in box. The single base mutation in the mutant is shown in shade.

To test whether the mutation was the reason for the *w81* mutant phenotype, a 7-kb wild type full-length complementary DNA containing the putative entire coding region, a 2.5-kb upstream sequence, and a 1-kb downstream sequence of LOC_Os05g50980 was introduced into the *w81* mutant. Five positive transgenic lines were obtained and identified by PCR. Those positive transgenic complementation lines generated normal green leaves and identical chlorophyll contents to the wild type, suggesting they completely rescued the *w81* mutant phenotypes (Figure 5A,B). To further confirm whether the disruption of LOC_Os05g50980 is responsible for the *w81* mutant phenotype, we constructed a LOC_Os05g50980 gene CRISPR vector and the knockout site was near the start codon of OsPAP7 and then transferred it to Japonica cultivar Kitaake (Figure 4D). However, the positive transgenic plant with a low-level expression of LOC_Os05g50980 presented white seedlings, which gradually withered to death (Figure 5C). These data revealed that LOC_Os05g50980 indeed corresponds to the *W81* gene. The full-length mRNA of LOC_Os05g50980 is 1434 bp, contains 11 exons and encodes a 478-amino acid SET domain-containing protein with an estimated molecular mass of approximately 55 kDa. It was designated as OsPAP7 from previous studies by sequence comparison [17,39].

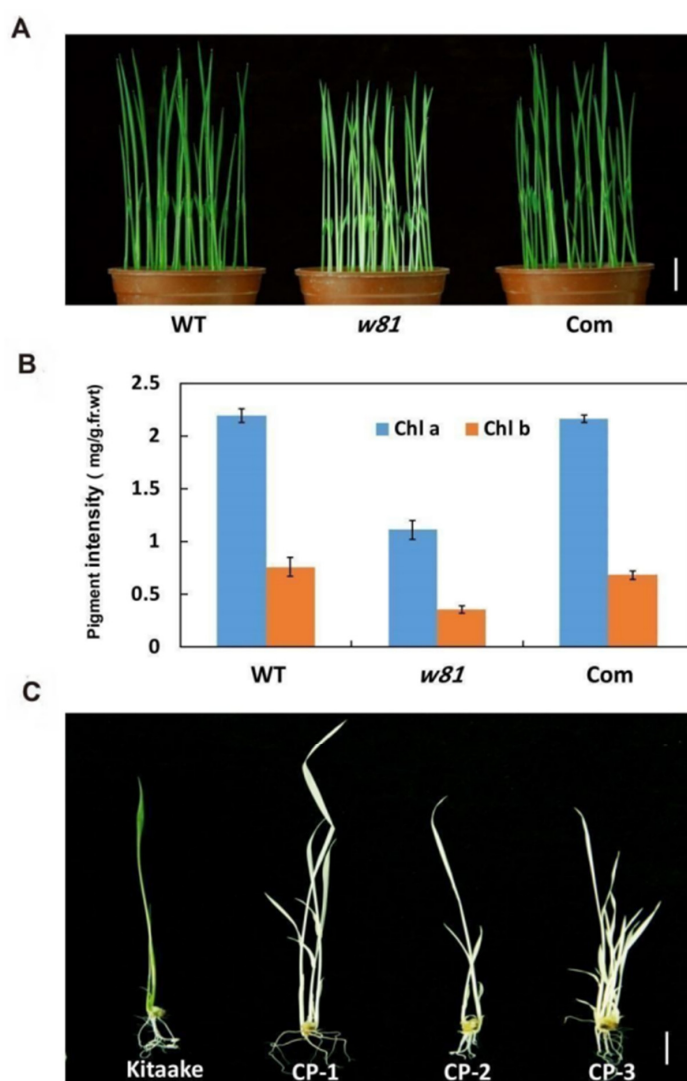


Figure 5. Complementation test of the *W81* gene. (A) Seedlings of the wild type (WT), *w81* mutant, and a complementary plant (Com). Scale bars = 2 cm. (B) The chlorophyll contents of the third leaf from the WT, *w81* mutant, and a complementary plant (Com) at the three-leaf stage. Fr.Wt: fresh weight; Chl a: Chlorophyll a; Chl b: Chlorophyll b. Error bars represent \pm SD ($n = 3$). (C) Phenotypic comparison of Kitaake and three *W81* gene CRISPR plant lines.

3.4. Bioinformatics Analysis and Subcellular Localization of OsPAP7

Sequence analysis showed that OsPAP7 contains two main domains: a SET domain and a Rubis-sub-bind domain (Figures A1 and A2B). The former may play a role in the transfer of methyl groups on target proteins [40], and the latter is for substrate/interactor binding. Ospap7, the putative protein in the *w81* mutant, may encode a truncated protein due to the abnormal splicing and a gain of premature termination codon (Figures 4E,F and A2A). The mutation version lacks 251 amino acid residues at the C-terminal, but remains a partial SET domain (Figure A2B), suggesting it may have partial transferase activity and is a leaky mutation. Protein sequence comparison and phylogenetic analysis revealed that PAP7 protein is highly conserved in plants and OsPAP7 has its close homologs in *Arabidopsis thaliana* (NP_193746.3; 72.2% similarity), *Zea mays* (NP_001146209.1; 89.3% similarity), *Brachypodium distachyon* (XP_003567801.1; 90.2% similarity), *Triticum urartu* (EMS60454.1; 79.4% similarity), *Sorghum bicolor* (XP_002440355.1; 89.0% similarity), *Setaria italica* (XP_004961052.1; 90.6% similarity; Figure A3). Among them, the *Arabidopsis* homolog NP_193746.3 (AtPAP7/AtPTAC14) has been identified to interact with pTAC12 and regulates plastid gene expression [24].

TargetP (<https://services.healthtech.dtu.dk/services/TargetP-2.0/>, accessed on 20 May 2023) predicted that OsPAP7 has a chloroplast transit peptide at its N-terminus, suggesting it may localize in chloroplasts. To verify this, we constructed an OsPAP7-GFP fusion protein and then transformed it into rice protoplasts. Chloroplast autofluorescence was used as a chloroplast marker to confirm OsPAP7 protein localization. A yellow signal was detected in the merged image, suggesting the OsPAP7 was co-localized with the chloroplast (Figure A2C). Meanwhile, we found that the Ospap7-GFP mutant fusion protein was also localized at the chloroplast (Figure A2C), indicating that the mutation in the *w81* mutant did not affect the protein localization. Our data suggest that the OsPAP7 protein is mainly localized in the chloroplast. Considering *Arabidopsis* PAPs (such as PAP5, PAP8, and PAP7) were reported to target both chloroplast and nuclear [41], we could not exclude that OsPAP7 is also dual targeting. This needs to be confirmed by using a Δ cTP version of OsPAP7 for the localization experiment, as described previously [41].

3.5. Expression Analysis of OsPAP7

To investigate the actual expression profile of *OsPAP7*, RNA samples from different tissues were analyzed, including culms (C), young leaves (YL), shoot base (SB), young panicles (P), young roots (R) at the seedling stage, and leaf sheaths (LS) at the booting stage by quantitative RT-PCR (qRT-PCR). The results showed that expression levels of *OsPAP7* in young leaves were substantially higher than other tissues examined (Figure 6A), which supports the hypothesis that *OsPAP7* is involved in rice chloroplast development in early leaf development.

To detect whether the light affects the expression of *OsPAP7*, we analyzed its expression using qRT-PCR during the greening of etiolated rice seedlings. After growing in darkness for 12 days, wild type seedlings were illuminated for varying times (3, 6, 9, 12, 15, 18, 21 and 24 h). The transcript level of *OsPAP7* was gradually increased and peaked at 9 h of illumination, after which it gradually decreased and reached rough equilibrium (Figure 6B). Together, these data suggest *OsPAP7* probably plays a significant role in light-induced rice chloroplast development in early leaf development.

3.6. Expression of Plastid- and Nuclear-Encoded Genes

Plastidic genes can be divided into three types: class I, class II and class III. Class I genes are transcribed by PEP, class III genes are transcribed by NEP and class II are transcribed by both NEP and PEP [11,12]. CAB1R, CAB2R, and *rbcS* are related to photosynthesis, and HEMA1 is required for chlorophyll biosynthesis. In order to further explore whether the functional deficiency of *OsPAP7* alters plastid- and chloroplast-localized nuclear-encoded gene expression, three types of plastidic genes were examined. Class I genes *psaA*, *psbA* and *rbcL*, class II genes *clpP* and *rrn16*, class III genes *rpoA*, *rpoB*, *rpoC1* and *rpoC2* and nuclear-

encoded genes *CAB1R*, *CAB2R*, *rbcS* and *HEMA1* were chosen for the analysis. As a result, the expression levels of chloroplast-localized nuclear-encoded genes (*CAB1R*, *CAB2R*, *rbcS* and *HEMA1*) were dramatically down-regulated in the *w81* mutant, indicating that the photosynthesis and chlorophyll biosynthesis were abnormal in the *w81* mutant (Figure 7). Meanwhile, the expression of PEP-dependent genes (class I genes *psaA*, *psbA*, *rbcL* and class II gene *rrn16*) was remarkably down-regulated, while expression of NEP-dependent genes (class III genes *rpoB*, *rpoC1*, *rpoC2* and class II gene *clpP*) was significantly up-regulated in the *w81* mutant (Figure 7). These transcription changes were mostly consistent with the previous study in the *Arabidopsis pap7* mutant [42]. These above analyses suggest that the functional deficiency of OsPAP7 alters the expression of plastid- and chloroplast-localized nuclear-encoded genes, and the PEP complex activity is blocked in the *w81* mutant.

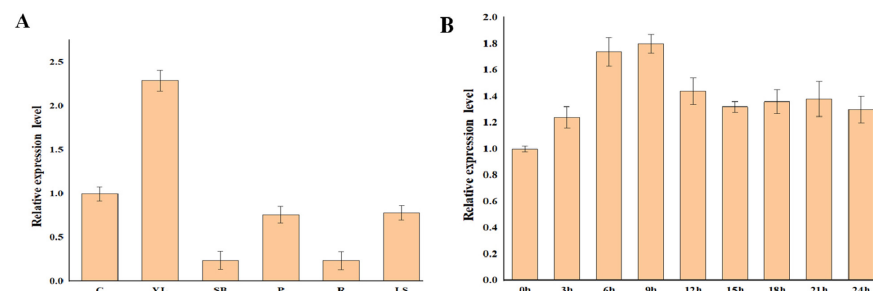


Figure 6. Gene expression of *OsPAP7*. (A) Relative expression of *W81* in culms (C), young leaves (YL), shoot base (SB), young panicles (P), young roots (R) and leaf sheaths (LS) from wild type plants. Values are mean \pm SD of three replicates. (B) qRT-PCR analysis of the *OsPAP7* gene during greening of etiolated rice seedlings. After growing in darkness for 12 days, wild type seedlings were illuminated for varying times (3, 6, 9, 12, 15, 18, 21 and 24 h). The ubiquitin gene was used as an internal control. The data were from three independent experiments, and error bars represent SD (\pm SD).

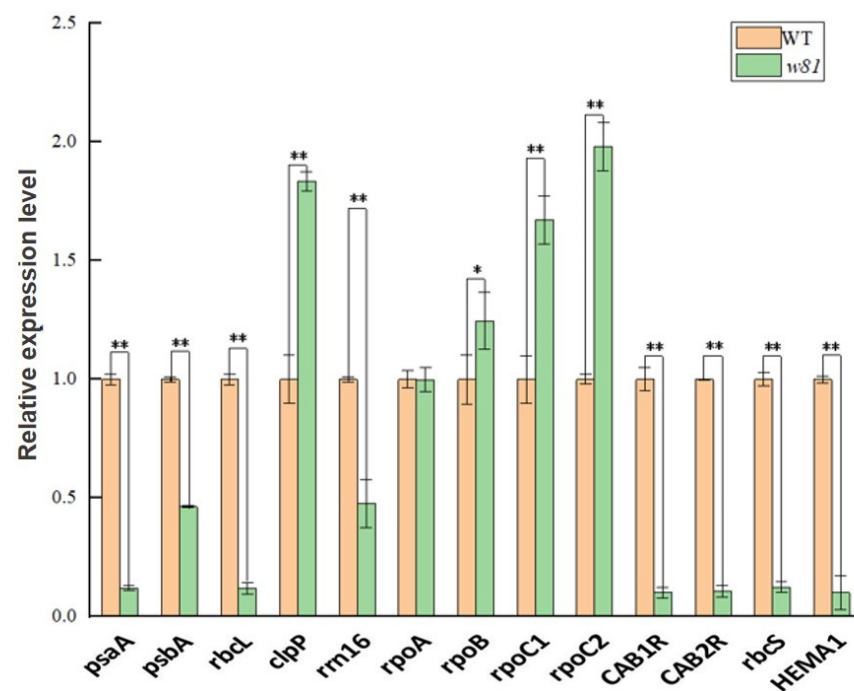


Figure 7. Expression of plastid- and nuclear-encoded genes. Quantitative RT-PCR analysis of plastid- and nuclear-encoded genes in WT and *w81* mutant. The RNA was isolated from the third leaves of the corresponding plants at the three-leaf stage. The tested genes were: *psaA*, *psbA*, *rbcL*, *clpP*, *rrn16*, *rpoA*, *rpoB*, *rpoC1*, *rpoC2*, *CAB1R*, *CAB2R*, *rbcS*, and *HEMA1*. Error bars represent \pm SD of three repeats. * $p < 0.05$; ** $p < 0.01$.

3.7. OsPAP7 Directly Interacts with OsPAP5

AtpTAC14, the homologous protein of OsPAP7 in *Arabidopsis*, has been reported to interact with AtpTAC12 (AtPAP5) in yeast [24]. Here a yeast two-hybrid assay was performed to identify the interaction between OsPAP7 and OsPAP5 in rice. Either OsPAP7 was fused to pGBK-T7 to generate a bait, and OsPAP5 was fused to pGAD-T7 to serve as prey or a reverse experiment in which OsPAP5 was fused to the binding domain of pGBK-T7, and OsPAP7 was fused to the activation domain of pGAD-T7. Results showed that OsPAP7 and OsPAP5 directly interact with each other (Figure 8A).

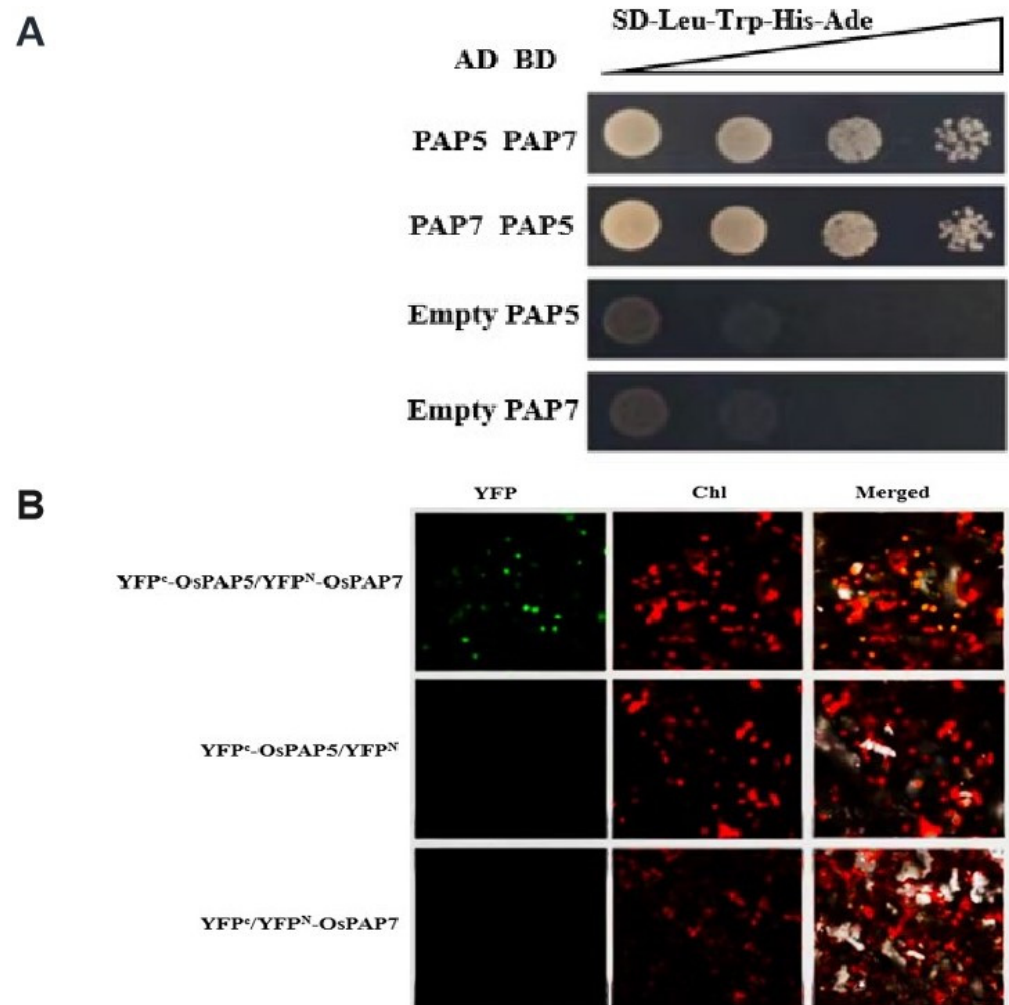


Figure 8. The interaction between OsPAP7 and OsPAP5. **(A)** Yeast two-hybrid assay of the interaction between OsPAP7 and other OsPAP5. **(B)** BiFC assay of the interaction between OsPAP7 and OsPAP5 in chloroplasts of tobacco leaf mesophyll cells.

To further verify the interaction between OsPAP7 and OsPAP5, bimolecular fluorescence complementation (BiFC) assays were performed. The amplified coding sequence of OsPAP7 and OsPAP5 were inserted into the BiFC vector to form YFP^C/YFP^N-OsPAP7 and YFP^C-OsPAP5/YFP^N, respectively. The sequence-validated vector was further used to construct the YFP^C-OsPAP5/YFP^N-OsPAP7 vector. The constructed BiFC vectors were transferred into yeast AH109 strain for transient expression into 6-week-old tobacco leaves as previously described. The BiFC data further confirmed that OsPAP7 directly interacts with OsPAP5 physically (Figure 8B).

4. Discussion

The main organs of photosynthesis in green plants are the leaves, which are also an important place for the synthesis of a variety of nutrients and secondary metabolites [43]. The symptom of most leaf color mutants emerges from the seedling stage and lasts until maturity. Consistently, the chlorophyll content was lower than that of normal green plants, and the height and 1000-grain weight of mature plants were also lower than the normal level [30,44]. However, the yellow-green leaf phenotype of the *w81* mutant in this study appeared from the seedling stage, peaked at the three-leaf stage, and then restored to green at the heading stage (Figure 1A–D). The chlorophyll content was significantly lower than that of the wild type before heading, but there was no significant difference after heading (Figure 1E). Interestingly, there was no significant difference in agronomic traits such as plant architecture and yield-related traits (Table A2). The phenotype of the *w81* mutant is similar to other reported late green-revertible rice mutants. The *white stripe leaf 7* (*wsl7*) is a low-temperature-induced mutant with an obvious phenotype in the early stage of vegetative growth and turns green in the later stage [45]. The rice white stripe mutant *wsl8* grows white leaves before the four-leaf stage, and afterward, the plants restore to normal green leaves [30]. The *gry3* mutant showed striped yellow leaves at the seedling stage and began to turn green at the late tillering stage until the heading stage [46]. The *ylws* mutant showed white-striped leaves at the growth stage of two- to four-leaf, and then the leaves gradually became green [44].

The *OsPAP7* expression level is the highest in young leaves, implying that *OsPAP7* plays a vital role in early chloroplast development and chlorophyll content. *Ospap7* in the *w81* mutant is a leaky mutation and might form a truncated protein; thus, it could remain a partial protein for enzymic function. Before the four-leaf stage, defective *OsPAP7* could not fully perform its molecular function in comparison to the wild type. However, when *OsPAP7* was down-regulated after the four-leaf stage, the defective *OsPAP7* with partial function was enough to recover early chloroplast development and chlorophyll content. Another explanation for leaf color recovery in the *w81* mutant is that other PAPs or factors might supplement the defective *OsPAP7* after the four-leaf stage. Moreover, some correctly spliced transcripts remaining in the *w81* mutant (Figure 4E) might be sufficient to restore the green-yellow phenotype.

ROS comprise many species, such as singlet oxygen (1O_2), superoxide anions (O_2^-), hydroxyl radicals ($\cdot OH$) and hydrogen peroxide (H_2O_2), which affect proteins, lipids and DNA repairment [47–49]. Plants have evolved effective mechanisms against ROS protection. Under suitable environmental conditions, plants produce the appropriate amount of ROS, which has no negative effect on plant growth. In this case, ROS are scavenged by antioxidant systems containing low molecular weight ascorbic acid (AsA) and glutamic acid (GSH), as well as antioxidant enzymes including catalase (CAT), superoxide dismutase (SOD), peroxidase (POX), and glutamyl glycine reductase (GR). However, under severe environmental stress, the delicate balance between ROS production and clearance is broken, resulting in ROS accumulation, which has a serious impact on photosynthesis systems and other cellular structures and processes [49–51]. Under photooxidation, the color of rice leaves will become lighter, and photooxidation will destroy the content and structure of chlorophyll. As a result, the light absorption capacity and rate of leaves decrease, which affects photosynthesis and leads to abnormal growth and development of plants [33]. Through NBT and DAB staining, we found that leaves of the *w81* mutant accumulate more reactive oxygen species compared with the wild type (Figure 3A,B). Through qRT-PCR, we found that the expression of antioxidant genes in the *w81* mutant was significantly increased (Figure 3C). These results suggest that the ROS scavenge system is activated at the transcription level.

PEP is a protein complex encoded by both plastid and nuclear genes and is the main RNA polymerase after chloroplast maturation. The regulation of PEP activity is by multiple genes [20,52]. *WSL3* encodes a subunit of plastid RNA polymerase *OsPAP1/OspTAC3*, which mutation is albino lethal and severely impaired PEP activity [53]. *OsCAF1* encodes

a chloroplast protein containing a CRM domain and is involved in the intron splicing of six plastid genes (*atpF*, *ndhA*, *ndhB*, *rpl2*, *rps12*, and *ycf3*). The *OsCAF1* mutant showed a significant decrease in albino lethality and PEP activity [54]. The mechanism of chloroplast transcription mediated by PEP is essential for high photo-efficiency and photosynthesis in plants [55,56]. Here we identified a novel PEP-related protein OsPAP7, which encoded a protein that mainly decreased the expression of genes related to chloroplast development and photosynthesis and increased the expression of genes encoded by NEP (Figure 7). This indicated that the loss of *OsPAP7* function changed the expression of genes encoded by both plastids and chloroplast nuclei and damaged the activity of the PEP complex.

In *Arabidopsis*, PAP7 has some nuclear localization signal (NLS), and it is chloroplast and nuclear dual targeting [10,41]. Through the comparison of *Arabidopsis* PAP7 and its homologs in the other species (Figure A1), OsPAP7 also contains two possible NLS sequences. Thus, further study needs to be conducted to verify the nuclear localization of OsPAP7. In addition, our study showed that OsPAP7 interacts with OsPAP5 (Figure 8). Previous research showed that *Arabidopsis* PAP7 interacts with PAP5, PAP8, and PAP12 in the cell nucleus. Whether the same interaction happens in rice cell nuclear needs further investigation in the future.

In summary, we found a novel gene controlling the yellow-green leaf phenotype in rice. This gene controls the leaf color at the heading stage with no observable impact on rice yield. Therefore, the yellow-green leaf phenotype can be utilized as an early visual marker to improve the purity of hybrid rice seeds and mechanized production. This gene reduces the expression of plastid genes transcribed by PEP. Considering that the protein function of the PEP complex has not been fully revealed in rice, this study provides a basis for a better understanding of chloroplast development and high photosynthesis capacity.

Author Contributions: Conceptualization, methodology, software, formal analysis, Y.W. (Ying Wang), S.S., X.D. (Xin Ding) and L.L.; investigation, Y.W. (Ying Wang), S.S., X.D. (Xin Ding), Y.T., Z.W., H.L., Q.L., Y.W. (Yunpeng Wang) and L.L.; validation, Y.W. (Ying Wang), X.D. (Xin Ding) and L.L.; resources, Y.W. (Ying Wang), S.Z. and L.L.; data curation, Y.W. (Ying Wang) and L.L.; writing—S.S., Y.W. (Ying Wang), L.L. and X.D. (Xiaoou Dong); visualization, S.S. and L.L.; supervision, J.W. and L.L.; project administration, J.W. and L.L.; funding acquisition, J.W. and L.L. All authors have read and agreed to the published version of the manuscript.

Funding: This study was funded by Jiangsu key R&D project (BE2021360), Yuan Long-Ping high tech, South Japonica rice research academy, Key Lab of Biology, Genetics and Breeding of Japonica Rice in Midlower Yangtze River, Ministry of Agriculture, P. R. China, Jiangsu Collaborative Innovation Center for Modern Crop Production.

Data Availability Statement: Data is contained within the article.

Conflicts of Interest: The authors declare no conflict of interest.

Appendix A

Table A1. List of primer pairs.

Name of Primer	Sequence (5'–3')
Primers for Map-Based Cloning	
S5-1-F	TCACATTGCCTCCAACAAAG
S5-1-R	TTCCCAGGTCGTTTGTTC
S5-26-F	TCAATAGGCCCAACCAAAAG
S5-26-R	AGTGACGCGATCTCCAATC
S5-16-F	ACATCGTACGTGTGCATGGT
S5-16-R	CGAATTCATCGTCTCCATC
S5-9-F	TCCATTCCACGTA CTGTTGC
S5-9-R	CACAAGGGGATTGAGGAGAA

Table A1. Cont.

Name of Primer	Sequence (5'–3')
Primers for Map-Based Cloning	
L5-8-F	TCTCCTTGGCCATCGTATTC
L5-8-R	GGCCGCATTTGTATGAAATC
S5-19-F	ATCTCCACCTACGCCCTCTT
S5-19-R	CTGTGGATCTCCTGCCTCTC
S5-3-F	CTTTGGTTTTGGTCGGTTGT
S5-3-R	TCTTGCCCTTGAGACATTT
980-J-3-F	AACTTCGCTGGCTTGGGTAC
980-J-3-R	ATCTCCTGGTCTTGTGAATAGTG
Primers for detecting transcripts	
980-CDS-CUT-1F	ATGGCGACTCCCCCGCT
980-CDS-CUT-1R	CTAAAACAAAATTTTATCCTGG
Primers for transgenic and CRISPR constructs	
w81-G-F	CCATGATTACGAATTCGTGGGGACAGGTTGAGTGG
w81-G-R	TACCGAGCTCGAATTCCTTCATCGCTGGGTTGTCG
CP-980-F	AGATGATCCGTGGCACCCCGACTTCTACCGGATGTTTTAGAGCTATGC
CP-980-R	GCATAGCTCTAAAACATCCGGTAGAAGTCGGGGTGCCACGGATCATCT
OsPAP7-GFP-InXbaI	CGGAGCTAGCTCTAGAATGGCGACTCCCGCCGCTTC
OsPAP7-GFP-InBamHI	TGCTCACCATGGATCCAAACAAAATTTTATCCTGGTAG
Ospap7-GFP-InXbaI	CGGAGCTAGCTCTAGAATGGCGACTCCCGCC
Ospap7-GFP-InBamHI	TGCTCACCATGGATCCAAATAGTACAGAAGTGATACC
Primers for Y2H	
BD-OsPAP7-F	CATGGAGGCCGAATTCATGGCGACTCCCGCCGCT
BD-OsPAP7-R	CAGGTTCGACGGATCCCCTAAAACAAAATTTTATCCT
BD-OsPAP5-F	CATGGAGGCCGAATTCATCCTGTCCCCTTCCGAA
BD-OsPAP5-R	CAGGTTCGACGGATCCCTCAGCAACTTGATCCTTATAT
AD-OsPAP1-F	CAGATTACGCTCATATGATGGCCACCCCTACCCCCAC
AD-OsPAP1-R	CACCCGGGTGGAATTCCTACTCCTCTGCAGGTGGCGGTT
AD-OsPAP2-F	CAGATTACGCTCATATGATGAAGGCCTCCGGCGTGC
AD-OsPAP2-R	CACCCGGGTGGAATTCACAGTGCAAGGAGTTCT
AD-OsPAP3-F	CAGATTACGCTCATATGATGGCGGCCACTCCGGCC
AD-OsPAP3-R	CACCCGGGTGGAATTCATTTGTGATGAAACAC
AD-OsPAP4-F	CAGATTACGCTCATATGATGGCGGCTTTCGCCTC
AD-OsPAP4-R	CACCCGGGTGGAATTCATGCAACTGGGATATTTGG
AD-OsPAP5-F	CAGATTACGCTCATATGATGGCGTCGTGCTCCCG
AD-OsPAP5-R	CACCCGGGTGGAATTCCTACTCATCTTCTTCGAAGTCCAT
AD-OsPAP6-F	CAGATTACGCTCATATGATGGCCATGGCGGCCTC
AD-OsPAP6-R	CACCCGGGTGGAATTCCTAGATGAAAACCATCCAGATAAT
AD-OsPAP7-F	CAGATTACGCTCATATGATGGCGACTCCCGCCG
AD-OsPAP7-R	CACCCGGGTGGAATTCCTAAAACAAAATTTTATCCTGGTAG
AD-OsPAP8-F	CAGATTACGCTCATATGATGGCGGCCACCGTGT
AD-OsPAP8-R	CACCCGGGTGGAATTCAGAACCAATTCGAGTAGTCAAAG
AD-OsPAP9-F	CAGATTACGCTCATATGATGGCGTTCGCCACACTG
AD-OsPAP9-R	CACCCGGGTGGAATTCACACCCCTAGGGACTTCTCT
AD-OsPAP10-F	CAGATTACGCTCATATGATGGCCATGGCCGCGG
AD-OsPAP10-R	CACCCGGGTGGAATTCACAATTCATTATCAATGATATTT
Primers for BiFC	
BiFC-N-PAP5-BamH-F	AACTAGTGGAGGATCCATGGCGTCGTGCTCCCGCA
BiFC-N-PAP5-BamH-R	ACCCACCTCCGGATCCCTCATCTTCTTCGAAGTCC
BiFC-C-PAP7-PmlI-F	CCTACGTAGTCACGTGATGGCGACTCCCGCCGCT
BiFC-C-PAP7-PmlI-R	CTCCGGACGTACAGTGAAACAAAATTTTATCCTGG
Primers for qRT-PCR	
OsPAP7-RT-F	CTTCTCGAGTGATGCCAAGA
OsPAP7-RT-R	ATGCAGCATTGTGGTAGAGC
HEMA1-F	CACCAGTCTGAATCATAT
HEMA1-R	CTACCACCTTCTCTAATCC

Table A1. Cont.

Name of Primer	Sequence (5'-3')
Primers for Map-Based Cloning	
<i>CAB1R-F</i>	AGACGTTCCGCAAGAACC
<i>CAB1R-R</i>	GAGGAGCTCCGGGAAGAC
<i>CAB2R-F</i>	GTTCTCCATGTTCCGGCTTCT
<i>CAB2R-R</i>	GACGAAGTTGGTGGCGTAG
<i>psaA-F</i>	GAGATACCACTTCCTCAT
<i>psaA-R</i>	ACTAAGAAATTCTGCGTATT
<i>psbA-F</i>	AAGTTTCTCTGATGGTATG
<i>psbA-R</i>	ATAGCACTGAATAGGGAA
<i>rbcS-F</i>	TCATCAGCTTCATCGCCTAC
<i>rbcS-R</i>	ACTGGGAACACACGAAACAA
<i>rbcL-F</i>	GTTGAAAGGGATAAGTTGA
<i>rbcL-R</i>	AATGGTTGTGAGTTTACG
<i>clpP-F</i>	GATACGATGCAAACGGTGAC
<i>clpP-R</i>	GGGAATGCTATACGCTTGGT
<i>rrn16-F</i>	GGAGAAGAAGCAATGACGGT
<i>rrn16-R</i>	GATCATTCCGGATAACGCTT
<i>rpoA-F</i>	AAATCGTTGATACGGCACAA
<i>rpoA-R</i>	ATTCACATTTGGAACAGGCA
<i>rpoB-F</i>	GCATTGTTGGAACTGGATTG
<i>rpoB-R</i>	GCCGATGGGTAACATAAAGGA
<i>rpoC1-F</i>	TTGTGGGTCCTTCACTTTCA
<i>rpoC1-R</i>	TTCCCATAACAATGGGTTCTT
<i>rpoC2-F</i>	GAGGACGAACATGGGACTTT
<i>rpoC2-R</i>	GTTCTCGATGCTCAATCAA
<i>Ubg-F</i>	GCTCCGTGGCGGTATCAT
<i>Ubg-R</i>	CGGCAGTTGACAGCCCTAG

Table A2. Statistics of major agronomic traits.

Genotype	Plant Height (cm)	Number of Tillers per Plant	Branch Number per Panicle	Number of Spikelets per Panicle	1000-Grain Weight (g)
Wild type	83.0 ± 3.4	9.9 ± 1.7	9.3 ± 1.6	122.8 ± 22.2	24.5 ± 0.1
<i>w81</i>	82.5 ± 2.9	8.9 ± 1.4	8.7 ± 1.4	123.2 ± 22.7	25.1 ± 0.1

Each value is mean ± SD from 30 plants.

Table A3. Genetic analysis of two F₂ populations.

Cross	Normal	Yellow	Ratio 3:1 ^a
Wild type	638	203	2.45
<i>w81</i>	577	189	1.49

^a Value for K-square test at $p = 0.05$ and 1 *df* is 3.84.

Appendix B

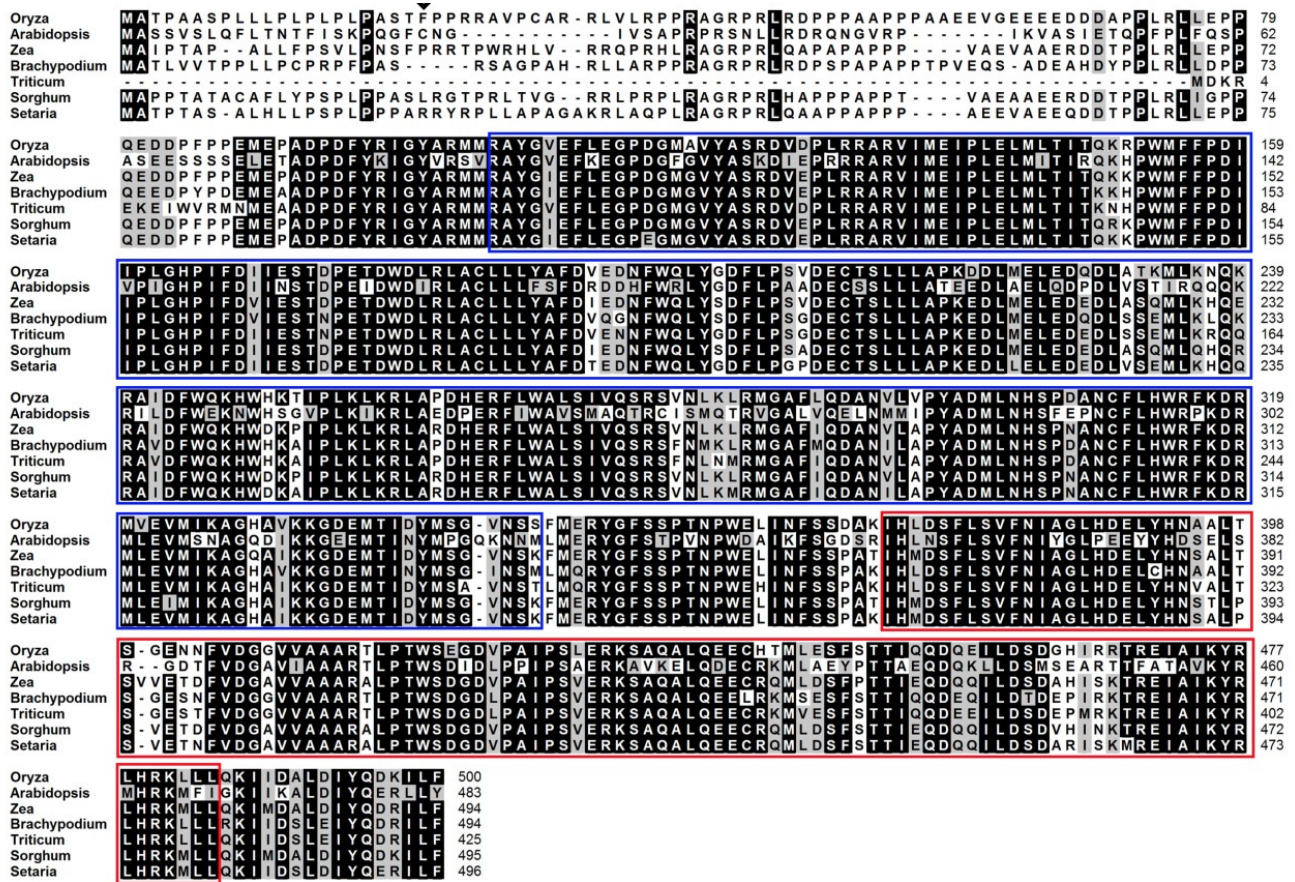


Figure A1. Amino acid sequence alignment of OsPAP7 homologs. Sequences are from *Oryza sativa* OsPAP7, *Arabidopsis thaliana* NP_193746.3, *Zea mays* NP_001146209.1, *Brachypodium distachyon* XP_003567801.1, *Triticum urartu* EMS60454.1, *Sorghum bicolor* XP_002440355.1, *Setaria italica* XP_004961052.1. Blue rectangle and red rectangle, respectively, denote the SET domain and the Rubis-sub-bind domain of the PAP7 protein.

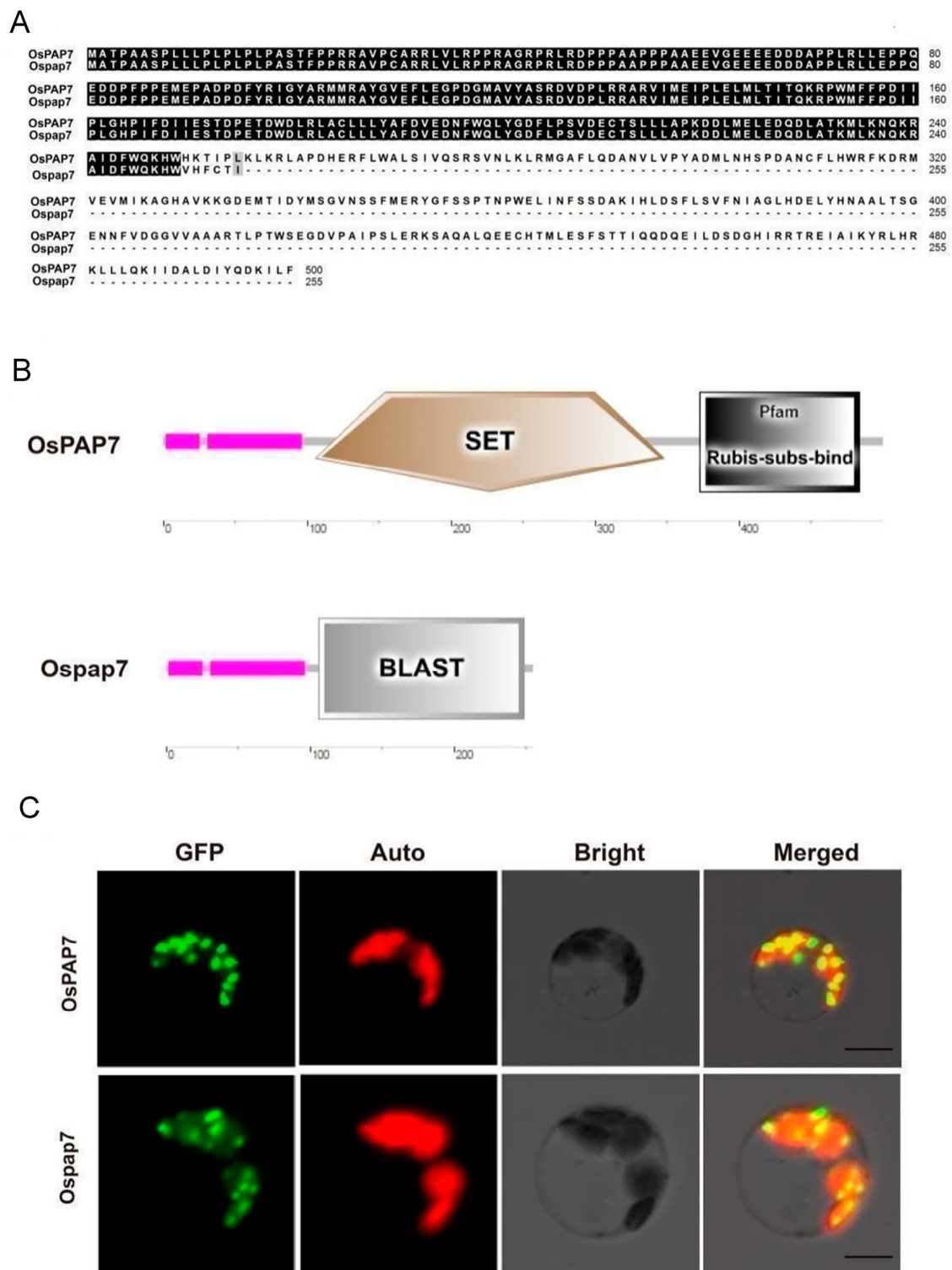


Figure A2. The difference of sequences and subcellular localization between OsPAP7 and Ospap7 protein. (A) Amino acid sequence alignment of OsPAP7 and Ospap7 protein. Compared to wild type OsPAP7 protein, the mis-splicing of *Ospap7* may result in a truncated protein losing 251 amino acid residues at the C-terminal. Ospap7, putative protein of the *w81* mutant. (B) OsPAP7 protein has a SET and a Rubis-sub-5-bind domain, whereas the Ospap7 protein has part of SET domain. (C) Transient expression of OsPAP7–GFP (upper panel) and Ospap7–GFP fusion proteins (lower panel) in rice protoplasts. GFP, GFP signals of OsPAP7 and Ospap7; Auto, Chl autofluorescence; Bright, bright field; Merged, merged images of GFP from Auto and Bright. Scale bars = 5µm.

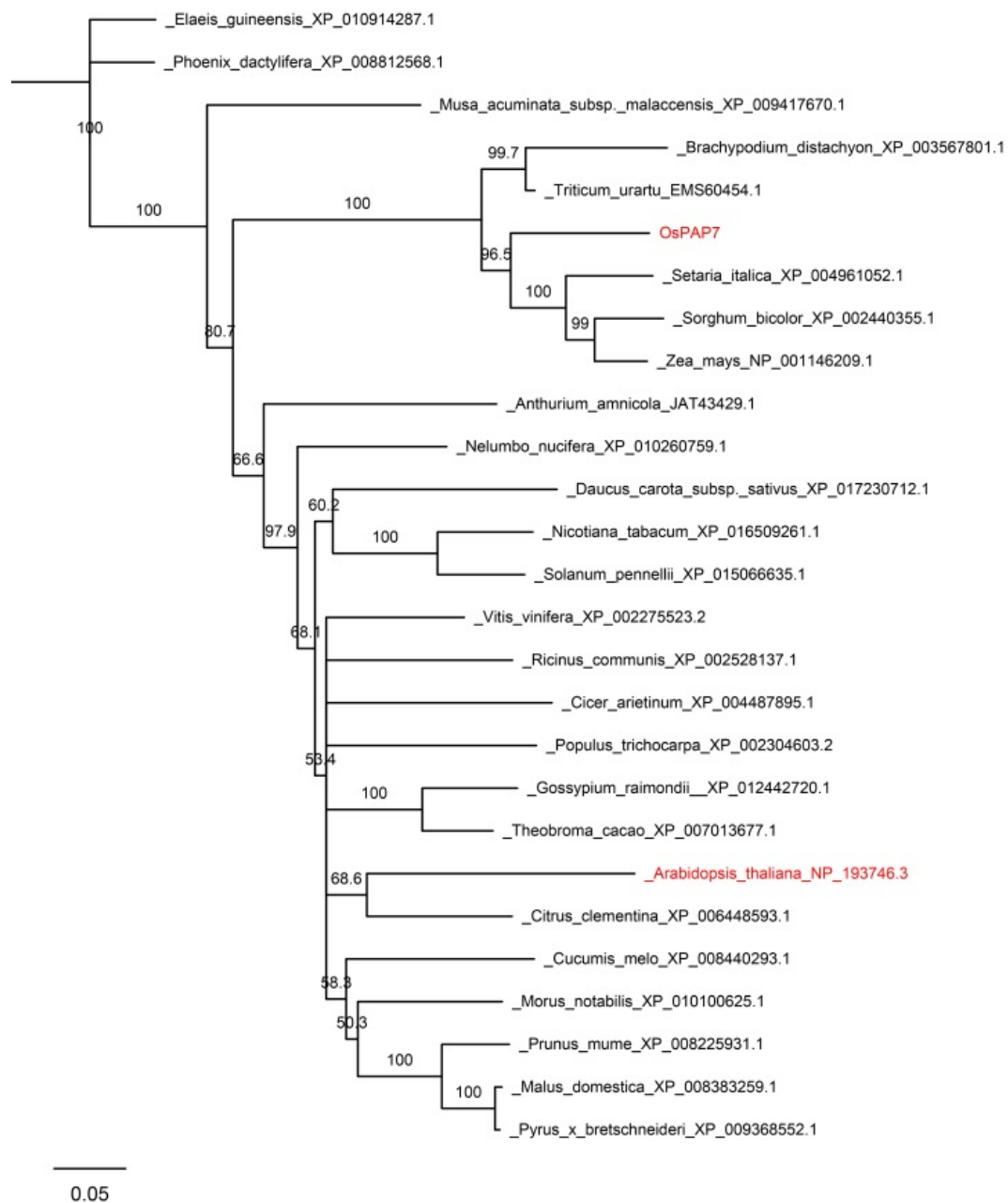


Figure A3. A phylogenetic tree of OsPAP7 in plants. The tree is constructed by MEGA X software. Numbers represent bootstrap values. The accession numbers are: XP_015637857.1 (*Oryza sativa Japonica* Group, in red), XP_003567801.1 (*Brachypodium distachyon*), XP_002440355.1 (*Sorghum bicolor*), NP_001146209.1 (*Zea mays*), XP_004961052.1 (*Setaria italica*), EMS60454.1 (*Triticum urartu*), XP_010914287.1 (*Elaeis guineensis*), XP_008812568.1 (*Phoenix dactylifera*), XP_008383259.1 (*Malus domestica*), XP_009368552.1 (*Pyrus x bretschneideri*), XP_009417670.1 (*Musa acuminata* subsp. *malaccensis*), XP_010260759.1 (*Nelumbo nucifera*), XP_002275523.2 (*Vitis vinifera*), XP_008225931.1 (*Prunus mume*), JAT43429.1 (*Anthurium amnicola*), XP_016558428.1 (*Capsicum annuum*), XP_016198002.1 (*Arachis ipaensis*), XP_008440293.1 (*Cucumis melo*), XP_006448593.1 (*Citrus clementina*), XP_016509261.1 (*Nicotiana tabacum*), XP_012442720.1 (*Gossypium raimondii*), XP_015875020.1 (*Gossypium jujuba*), XP_011096855.1 (*Sesamum indicum*), XP_012829685.1 (*Erythranthe guttata*), XP_004295521.2 (*Fragaria vesca* subsp. *vesca*), XP_010100625.1 (*Morus notabilis*), XP_002528137.1 (*Ricinus communis*), XP_015066635.1 (*Solanum pennellii*), XP_017230712.1 (*Daucus carota* subsp. *sativus*), XP_007013677.1 (*Theobroma cacao*), XP_002304603.2 (*Populus trichocarpa*), XP_012065975.1 (*Jatropha curcas*), XP_004487895.1 (*Cicer arietinum*), NP_193746.3 (*Arabidopsis thaliana*, in red).

References

1. Miyoshi, K.; Ito, Y.; Serizawa, A.; Kurata, N. *OsHAP3* genes regulate chloroplast biogenesis in rice. *Plant J.* **2003**, *36*, 532–540. [[CrossRef](#)]
2. Gothandam, K.M.; Kim, E.-S.; Cho, H.; Chung, Y.-Y. OsPPR1, a pentatricopeptide repeat protein of rice is essential for the chloroplast biogenesis. *Plant Mol. Biol.* **2005**, *58*, 421–433. [[CrossRef](#)]
3. Lv, Y.S.; Shao, G.N.; Qiu, J.H.; Jiao, G.A.; Sheng, Z.H.; Xie, L.H.; Wu, Y.W.; Tang, S.Q.; Wei, X.J.; Hu, P.S. White Leaf and Panicle 2, encoding a PEP-associated protein, is required for chloroplast biogenesis under heat stress in rice. *J. Exp. Bot.* **2017**, *68*, 5147–5160. [[CrossRef](#)] [[PubMed](#)]
4. Wang, Y.; Ren, Y.L.; Zhou, K.N.; Liu, L.L.; Wang, J.L.; Xu, Y.; Zhang, H.; Zhang, L.; Feng, Z.M.; Wang, L.W.; et al. *WHITE STRIPE LEAF4* encodes a novel p-type ppr protein required for chloroplast biogenesis during early leaf development. *Front. Plant Sci.* **2017**, *8*, 1116. [[CrossRef](#)]
5. Liu, Z.W.; Wang, Z.Y.; Gu, H.; You, J.; Hu, M.M.; Zhang, Y.J.; Zhu, Z.; Wang, Y.H.; Liu, S.J.; Chen, L.M.; et al. Identification and phenotypic characterization of ZEBRA LEAF16 encoding a β -Hydroxyacyl-ACP dehydratase in rice. *Front. Plant Sci.* **2018**, *9*, 782. [[CrossRef](#)]
6. Lee, S.; Joung, Y.H.; Kim, J.-K.; Choi, Y.D.; Jang, G. An isoform of the plastid RNA polymerase associated protein FSD3 negatively regulates chloroplast development. *BMC Plant Biol.* **2019**, *19*, 524. [[CrossRef](#)] [[PubMed](#)]
7. Liebers, M.; Cozzi, C.; Uecker, F.; Chambon, L.; Blanvillain, R.; Pfannschmidt, T. Biogenic signals from plastids and their role in chloroplast development. *J. Exp. Bot.* **2022**, *73*, 7105–7125. [[CrossRef](#)] [[PubMed](#)]
8. Hajdukiewicz, P.T.; Allison, L.A.; Maliga, P. The two RNA polymerases encoded by the nuclear and the plastid compartments transcribe distinct groups of genes in tobacco plastids. *EMBO J.* **1997**, *16*, 4041–4048. [[CrossRef](#)]
9. Liere, K.; Weihe, A.; Börner, T. The transcription machineries of plant mitochondria and chloroplasts: Composition, function, and regulation. *J. Plant Physiol.* **2011**, *168*, 1345–1360. [[CrossRef](#)]
10. Pfannschmidt, T.; Blanvillain, R.; Merendino, L.; Courtis, F.; Chevalier, F.; Liebers, M.; Grübler, B.; Hommel, E.; Lerbs-Mache, S. Plastid RNA polymerases: Orchestration of enzymes with different evolutionary origins controls chloroplast biogenesis during the plant life cycle. *J. Exp. Bot.* **2015**, *66*, 6957–6973. [[CrossRef](#)]
11. Hedtke, B.; Börner, T.; Weihe, A. Mitochondrial and chloroplast phage-type RNA polymerases in *Arabidopsis*. *Science* **1997**, *277*, 809–811. [[CrossRef](#)]
12. Yu, Q.-B.; Huang, C.; Yang, Z.-N. Nuclear-encoded factors associated with the chloroplast transcription machinery of higher plants. *Front. Plant Sci.* **2014**, *5*, 316. [[CrossRef](#)]
13. Zhelyazkova, P.; Sharma, C.M.; Förstner, K.U.; Liere, K.; Vogel, J.; Börner, T. The primary transcriptome of barley chloroplasts: Numerous noncoding RNAs and the dominating role of the plastid-encoded RNA polymerase. *Plant Cell* **2012**, *24*, 123–136. [[CrossRef](#)]
14. Börner, T.; Aleynikova, A.Y.; Zubo, Y.O.; Kusnetsov, V.V. Chloroplast RNA polymerases: Role in chloroplast biogenesis. *Biochim. Biophys. Acta* **2015**, *1847*, 761–769. [[CrossRef](#)]
15. Legen, J.; Kemp, S.; Krause, K.; Profanter, B.; Herrmann, R.G.; Maier, R.M. Comparative analysis of plastid transcription profiles of entire plastid chromosomes from tobacco attributed to wild-type and PEP-deficient transcription machineries. *Plant J.* **2002**, *31*, 171–188. [[CrossRef](#)]
16. Pfalz, J.; Pfannschmidt, T. Essential nucleoid proteins in early chloroplast development. *Trends Plant Sci.* **2013**, *18*, 186–194. [[CrossRef](#)]
17. Steiner, S.; Schröter, Y.; Pfalz, J.; Pfannschmidt, T. Identification of essential subunits in the plastid-encoded RNA polymerase complex reveals building blocks for proper plastid development. *Plant Physiol.* **2011**, *157*, 1043–1055. [[CrossRef](#)]
18. Majeran, W.; Friso, G.; Asakura, Y.; Qu, X.; Huang, M.; Ponnala, L.; Watkins, K.P.; Barkan, A.; van Wijk, K.J. Nucleoid-enriched proteomes in developing plastids and chloroplasts from maize leaves: A new conceptual framework for nucleoid functions. *Plant Physiol.* **2012**, *158*, 156–189. [[CrossRef](#)]
19. Melonek, J.; Oetke, S.; Krupinska, K. Multifunctionality of plastid nucleoids as revealed by proteome analyses. *Biochim. Biophys. Acta* **2016**, *1864*, 1016–1038. [[CrossRef](#)]
20. Pfalz, J.; Liere, K.; Kandlbinder, A.; Dietz, K.-J.; Oelmüller, R. pTAC2, -6, and -12 Are Components of the Transcriptionally Active Plastid Chromosome That Are Required for Plastid Gene Expression. *Plant Cell* **2005**, *18*, 176–197. [[CrossRef](#)]
21. Ji, Y.; Lehotai, N.; Zan, Y.J.; Dubreuil, C.; Díaz, M.G.; Strand, Å. A fully assembled plastid-encoded RNA polymerase complex detected in etioplasts and proplastids in *Arabidopsis*. *Physiol. Plant.* **2021**, *171*, 435–446. [[CrossRef](#)] [[PubMed](#)]
22. Yagi, Y.; Ishizaki, Y.; Nakahira, Y.; Tozawa, Y.; Shiina, T. Eukaryotic-type plastid nucleoid protein pTAC3 is essential for transcription by the bacterial-type plastid RNA polymerase. *Proc. Natl. Acad. Sci. USA* **2012**, *109*, 7541–7546. [[CrossRef](#)] [[PubMed](#)]
23. Myouga, F.; Hosoda, C.; Umezawa, T.; Iizumi, H.; Kuromori, T.; Motohashi, R.; Shono, Y.; Nagata, N.; Ikeuchi, M.; Shinozaki, K. A hetero complex of iron superoxide dismutases defends chloroplast nucleoids against oxidative stress and is essential for chloroplast development in *Arabidopsis*. *Plant Cell* **2008**, *20*, 3148–3162. [[CrossRef](#)]
24. Gao, Z.P.; Yu, Q.B.; Zhao, T.T.; Ma, Q.; Chen, G.X.; Yang, Z.N. A functional component of the transcriptionally active chromosome complex, *Arabidopsis* pTAC14, interacts with pTAC12/HEMERA and regulates plastid gene expression. *Plant Physiol.* **2011**, *157*, 1733–1745. [[CrossRef](#)] [[PubMed](#)]

25. Arsova, B.; Hoja, U.; Wimmelbacher, M.; Greiner, E.; Üstün, Ş.; Melzer, M.; Petersen, K.; Lein, W.; Börnke, F. Plastidial thioredoxin *z* interacts with two fructokinase-like proteins in a thiol-dependent manner: Evidence for an essential role in chloroplast development in *Arabidopsis* and *Nicotiana benthamiana*. *Plant Cell* **2010**, *22*, 1498–1515. [[CrossRef](#)]
26. Huang, C.; Yu, Q.-B.; Lv, R.-H.; Yin, Q.-Q.; Chen, G.-Y.; Xu, L.; Yang, Z.-N. The reduced plastid-encoded polymerase-dependent plastid gene expression leads to the delayed greening of the *Arabidopsis fln2* mutant. *PLoS ONE* **2013**, *8*, e73092. [[CrossRef](#)]
27. Yu, Q.-B.; Lu, Y.; Ma, Q.; Zhao, T.-T.; Huang, C.; Zhao, H.-F.; Zhang, X.-L.; Lv, R.-H.; Yang, Z.-N. TAC7, an essential component of the plastid transcriptionally active chromosome complex, interacts with FLN1, TAC10, TAC12 and TAC14 to regulate chloroplast gene expression in *Arabidopsis thaliana*. *Physiol. Plant.* **2012**, *148*, 408–421. [[CrossRef](#)]
28. Chang, S.H.; Lee, S.; Um, T.Y.; Kim, J.-K.; Choi, Y.D.; Jang, G. pTAC10, a Key Subunit of Plastid-Encoded RNA Polymerase, Promotes Chloroplast Development. *Plant Physiol.* **2017**, *174*, 435–449. [[CrossRef](#)]
29. Pfalz, J.; Holtzegel, U.; Barkan, A.; Weisheit, W.; Mittag, M.; Pfannschmidt, T. ZmpTAC12 binds single-stranded nucleic acids and is essential for accumulation of the plastid-encoded polymerase complex in maize. *New Phytol.* **2015**, *206*, 1024–1037. [[CrossRef](#)]
30. Liu, L.L.; You, J.; Zhu, Z.; Chen, K.Y.; Hu, M.M.; Gu, H.; Liu, Z.W.; Wang, Z.Y.; Wang, Y.H.; Liu, S.J.; et al. WHITE STRIPE LEAF8, encoding a deoxyribonucleoside kinase, is involved in chloroplast development in rice. *Plant Cell Rep.* **2020**, *39*, 19–33. [[CrossRef](#)]
31. Arnon, D.I. Copper enzymes in isolated chloroplasts. Polyphenoloxidase in *Beta vulgaris*. *Plant Physiol.* **1949**, *24*, 1–15. [[CrossRef](#)] [[PubMed](#)]
32. Zhou, K.; Ren, Y.; Lv, J.; Wang, Y.; Liu, F.; Zhou, F.; Zhao, S.; Chen, S.; Peng, C.; Zhang, X.; et al. Young Leaf Chlorosis 1, a chloroplast-localized gene required for chlorophyll and lutein accumulation during early leaf development in rice. *Planta* **2013**, *237*, 279–292. [[CrossRef](#)] [[PubMed](#)]
33. Wu, Z.; Zhang, X.; He, B.; Diao, L.; Sheng, S.; Wang, J.; Guo, X.; Su, N.; Wang, L.; Jiang, L.; et al. A Chlorophyll-Deficient Rice Mutant with Impaired Chlorophyllide Esterification in Chlorophyll Biosynthesis. *Plant Physiol.* **2007**, *145*, 29–40. [[CrossRef](#)]
34. Hiei, Y.; Ohta, S.; Komari, T.; Kumashiro, T. Efficient transformation of rice (*Oryza sativa* L.) mediated by *Agrobacterium* and sequence analysis of the boundaries of the T-DNA. *Plant J.* **1994**, *6*, 271–282. [[CrossRef](#)] [[PubMed](#)]
35. Waadt, R.; Kudla, J. In *Planta Visualization of Protein Interactions Using Bimolecular Fluorescence Complementation (BiFC)*. *CSH Protoc.* **2008**, *2008*, pdb.prot4995. [[CrossRef](#)]
36. Yoo, S.-D.; Cho, Y.-H.; Sheen, J. *Arabidopsis* mesophyll protoplasts: A versatile cell system for transient gene expression analysis. *Nat. Protoc.* **2007**, *2*, 1565–1572. [[CrossRef](#)]
37. Livak, K.; Schmittgen, T. Analysis of relative gene expression data using real-time quantitative PCR and the $2^{-\Delta\Delta CT}$ method. *Methods* **2001**, *25*, 402–408. [[CrossRef](#)]
38. Kang, S.G.; Lee, K.E.; Singh, M.; Kumar, P.; Matin, M.N. Rice lesion mimic mutants (LMM): The current understanding of genetic mutations in the failure of ROS scavenging during lesion formation. *Plants* **2021**, *10*, 1598. [[CrossRef](#)]
39. Garcia, M.; Myouga, F.; Takechi, K.; Sato, H.; Nabeshima, K.; Nagata, N.; Takio, S.; Shinozaki, K.; Takano, H. An *Arabidopsis* homolog of the bacterial peptidoglycan synthesis enzyme MurE has an essential role in chloroplast development. *Plant J.* **2008**, *53*, 924–934. [[CrossRef](#)]
40. Liebers, M.; Gillet, F.X.; Israel, A.; Pounot, K.; Chambon, L.; Chieb, M.; Chevalier, F.; Ruedas, R.; Favier, A.; Gans, P.; et al. Nucleo-plastidic PAP8/pTAC6 couples chloroplast formation with photomorphogenesis. *EMBO J.* **2020**, *39*, e104941. [[CrossRef](#)]
41. Chambon, L.; Gillet, F.-X.; Chieb, M.; Cobessi, D.; Pfannschmidt, T.; Blanvillain, R. PAP8/pTAC6 is part of a nuclear protein complex and displays rna recognition motifs of viral origin. *Int. J. Mol. Sci.* **2022**, *23*, 3059. [[CrossRef](#)]
42. Grübler, B.; Merendino, L.; Twardziok, S.O.; Mininno, M.; Allorent, G.; Chevalier, F.; Liebers, M.; Blanvillain, R.; Mayer, K.F.X.; Lerbs-Mache, S.; et al. Light and plastid signals regulate different sets of genes in the albino mutant *Pap7-1*. *Plant Physiol.* **2017**, *175*, 1203–1219. [[CrossRef](#)] [[PubMed](#)]
43. Leister, D. Chloroplast research in the genomic age. *Trends Genet.* **2003**, *19*, 47–56. [[CrossRef](#)] [[PubMed](#)]
44. Lan, J.; Lin, Q.; Zhou, C.; Liu, X.; Miao, R.; Ma, T.; Chen, Y.; Mou, C.; Jing, R.; Feng, M.; et al. Young Leaf White Stripe encodes a P-type PPR protein required for chloroplast development. *J. Integr. Plant Biol.* **2023**. [[CrossRef](#)] [[PubMed](#)]
45. Wang, Z.Y.; Liu, Z.W.; Gu, H. Phenotypic identification and candidate gene analysis of rice white stripe leaf mutant *wsl7*. *J. Nanjing Agric. Univ.* **2019**, *42*, 21–29.
46. Jiang, H.; Zhang, A.; Ruan, B.; Hu, H.; Guo, R.; Chen, J.; Qian, Q.; Gao, Z. Identification of Green-Revertible Yellow 3 (GRY3), encoding a 4-hydroxy-3-methylbut-2-enyl diphosphate reductase involved in chlorophyll synthesis under high temperature and high light in rice. *Crops J.* **2023**, *in press*. [[CrossRef](#)]
47. Foyer, C.H.; Lopez-Delgado, H.; Dat, J.F.; Scott, I.M. Hydrogen peroxide- and glutathione-associated mechanisms of acclimatory stress tolerance and signalling. *Physiol. Plant.* **1997**, *100*, 241–254. [[CrossRef](#)]
48. Suzuki, N.; Koussevitzky, S.; Mittler, R.; Miller, G. ROS and redox signalling in the response of plants to abiotic stress. *Plant Cell Environ.* **2012**, *35*, 259–270. [[CrossRef](#)]
49. Saed-Moucheshi, A.; Shekoofa, A.; Pessaraki, M. Reactive Oxygen Species (ROS) Generation and Detoxifying in Plants. *J. Plant Nutr.* **2014**, *37*, 1573–1585. [[CrossRef](#)]
50. Mittler, R.; Vanderauwera, S.; Suzuki, N.; Miller, G.; Tognetti, V.B.; Vandepoole, K.; Gollery, M.; Shulaev, V.; Breusegem, V.F. ROS signaling: The new wave? *Trends Plant Sci.* **2011**, *16*, 300–309. [[CrossRef](#)]
51. Lu, T.; Meng, Z.; Zhang, G.; Qi, M.; Sun, Z.; Liu, Y.; Li, T. Sub-high Temperature and High Light Intensity Induced Irreversible Inhibition on Photosynthesis System of Tomato Plant (*Solanum lycopersicum* L.). *Front. Plant Sci.* **2017**, *8*, 365. [[CrossRef](#)]

52. Kremnev, D.; Strand, A. Plastid encoded RNA polymerase activity and expression of photosynthesis genes required for embryo and seed development in Arabidopsis. *Front. Plant Sci.* **2014**, *5*, 385. [[CrossRef](#)] [[PubMed](#)]
53. Wang, L.; Wang, C.; Wang, Y.; Niu, M.; Ren, Y.; Zhou, K.; Zhang, H.; Lin, Q.; Wu, F.; Cheng, Z.; et al. WSL3, a component of the plastid-encoded plastid RNA polymerase, is essential for early chloroplast development in rice. *Plant Mol. Biol.* **2016**, *92*, 581–595. [[CrossRef](#)] [[PubMed](#)]
54. Zhang, Q.; Shen, L.; Wang, Z.; Hu, G.; Ren, D.; Hu, J.; Zhu, L.; Gao, Z.; Zhang, G.; Guo, L.; et al. OsCAF1, a CRM Domain Containing Protein, Influences Chloroplast Development. *Int. J. Mol. Sci.* **2019**, *20*, 4386. [[CrossRef](#)] [[PubMed](#)]
55. Demarsy, E.; Courtois, F.; Azevedo, J.; Buhot, L.; Lerbs-Mache, S. Building Up of the Plastid Transcriptional Machinery during Germination and Early Plant Development. *Plant Physiol.* **2006**, *142*, 993–1003. [[CrossRef](#)] [[PubMed](#)]
56. Kusumi, K.; Iba, K. Establishment of the chloroplast genetic system in rice during early leaf development and at low temperatures. *Front. Plant Sci.* **2014**, *5*, 386. [[CrossRef](#)]

Disclaimer/Publisher's Note: The statements, opinions and data contained in all publications are solely those of the individual author(s) and contributor(s) and not of MDPI and/or the editor(s). MDPI and/or the editor(s) disclaim responsibility for any injury to people or property resulting from any ideas, methods, instructions or products referred to in the content.